



저작자표시-비영리-변경금지 2.0 대한민국

이용자는 아래의 조건을 따르는 경우에 한하여 자유롭게

- 이 저작물을 복제, 배포, 전송, 전시, 공연 및 방송할 수 있습니다.

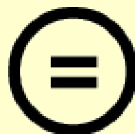
다음과 같은 조건을 따라야 합니다:



저작자표시. 귀하는 원저작자를 표시하여야 합니다.



비영리. 귀하는 이 저작물을 영리 목적으로 이용할 수 없습니다.




변경금지. 귀하는 이 저작물을 개작, 변형 또는 가공할 수 없습니다.

- 귀하는, 이 저작물의 재이용이나 배포의 경우, 이 저작물에 적용된 이용허락조건을 명확하게 나타내어야 합니다.
- 저작권자로부터 별도의 허가를 받으면 이러한 조건들은 적용되지 않습니다.

저작권법에 따른 이용자의 권리는 위의 내용에 의하여 영향을 받지 않습니다.

이것은 [이용허락규약\(Legal Code\)](#)을 이해하기 쉽게 요약한 것입니다.

[Disclaimer](#) 

Master's Thesis

Understanding dynamics of pure ring polymer in
the melt systems: Molecular Dynamics (MD)
Simulations in both 2-Dimension and 3-Dimension

Tae Hee Lee

School of Molecular Sciences
(Chemical Engineering)

Graduate School of UNIST

2016

**Understanding dynamics of pure ring polymer in
the melt systems: Molecular Dynamics (MD)
Simulations in both 2-Dimension and 3-Dimension**

Tae Hee Lee

School of Molecular Sciences
(Chemical Engineering)

Graduate School of UNIST

Understanding dynamics of pure ring polymer in the melt systems: Molecular Dynamics (MD) Simulations in both 2-Dimension and 3-Dimension

A thesis

submitted to the Graduate School of UNIST

in partial fulfillment of the
requirements for the degree of
Master of Science

Tae Hee Lee

1. 13. 2016

Approved by

Advisor

Chunggi Baig

Understanding dynamics of pure ring polymer in the melt systems: Molecular Dynamics (MD) Simulations in both 2-Dimension and 3-Dimension

Tae Hee Lee

This certifies that the thesis of Tae Hee Lee is
approved.

1. 13. 2016

signature

Advisor: Chunggi Baig

signature

Sang Kyu Kwak: Thesis Committee Member #1

signature

So Youn Kim: Thesis Committee Member #2

Abstract

The internally closed-loop molecular architecture without chain ends of ring polymers overall makes a significant influence on structural and dynamical properties of ring systems. In particular, ring polymer melts is known to exhibit a collapsed chain structure in the limit of long chain length. This is ascribed to an effective pressure acting on individual ring molecules via intermolecular topological interactions under the unknotted and uncrossability (or nonconcatenation) conditions. In addition, there has been a supposition in the community on the effect of interchain penetration on the rheological behaviors of ring melts. These two factors may play a key role in determining ring polymer rheology.

In this study, we investigated a direct correlation between the topological influence leading to a compact structure and dynamics of ring polymers, separately from the interchain penetration effect. To this, we first analyzed the structural and dynamical properties of ring polymer melts in 3-dimensional (3D) space by using molecular dynamics (MD) simulations implemented with an accurate united-atom model and a well-known coarse-grained Kremer-Grest model. These results show the general rheological behaviors of ring polymers in the melt. Second, we conducted 2-dimensional (2D) MD simulations of ring melts to exclude the interchain penetration effect, with all other conditions being preserved similar to the 3D melt systems. The topological effect resulting in a collapsed structure was found to become much more prominent for 2D systems, as compared to 3D systems: Flory's scaling exponent approaches to 1/2 and 1/3 for 2D and 3D systems, respectively.

2D ring polyethylene melts ranging from $C_{50}H_{100}$ to $C_{500}H_{1000}$ of molecular weight have been subjected to extensive atomistic MD simulations while the chain length in the Kremer-Grest 2D systems ranges from 30 beads up to 400 beads. We found that the 2D ring melts display distinctive scaling behaviors in dynamical properties; e.g., the longest relaxation time $\tau \sim N^\alpha$ with $\alpha \approx 2$ and the chain center-of-mass diffusion coefficient $D_{cm} \sim N^\beta$ with $-1 \leq \beta$, as compared with the corresponding results $2 \leq \alpha$ and $-2.4 \leq \beta \leq -1$ for 3D ring melts which have intermediate length. On the basis of the results of 2D ring systems possessing considerably collapsed structures even at moderate chain lengths, we may further predict the rheological behaviors of 3D ring melts of large chain lengths.

Contents

I. Introduction

II. Simulation method

2.1 United-atom model

2.2 Kremer-Grest model

2.3 Simulation details

III. Results and Discussion

3.1 Static and dynamic properties in 3D comparing with linear polymer

3.2 Static and dynamic properties in monolayer and strict 2D

3.3 Expectation of 3D large ring polymer dynamics

IV. Conclusion

List of figures

Figure 2.1.1 (a) Red atom represent united-atom1 (CH₂) and Blue atom represent united-atom2 (CH₃)

(b) polymer chains were connected by intramolecular potentials (stretching, bending, torsional, 6-12 Lennard-Jones).

Figure 1.2.1 (a) Purple bead represent Kremer-Grest bead (b) Kremer-Grest chain were connected by intramolecular potentials (FENE, WCA)

Figure 2.2.2 (a) general wall each wall, atoms were connected at reasonable distance (b) ideal smooth wall, atoms were connected infinitely short distance (c) polymer chains were confined between top and bottom ideal smooth wall

Figure 2.3.1 Density of 2D systems converges between 0.5~0.6 values relatively lower than 3D systems

Figure 2.3.2 (a) united-atom model in monolayer xy-plane (b) united-atom model in monolayer xz-plane (c) Kremer-Grest model in 2D xy-plane (d) Kremer-Grest model in 2D xz-plane

Figure 2.3.3 (a) knotted structure (b) concatenated structure (c) collapsed effect by surrounding chains (d) penetrated effect by surrounding chains

Figure 3.1.1 $\langle R_g^2 \rangle_{\text{linear}}$ and $\langle R_g^2 \rangle_{\text{ring}}$ in *NVT* MC simulation, these data were made using Suzuki et al. [ref] ring polymer ranging 10 to 1000 beads and linear polymer ranging 10 to 512

Figure 3.1.2 (a) $\langle R_g^2 \rangle_{\text{linear}}$ and $\langle R_g^2 \rangle_{\text{ring}}$ in *NPT* MD simulation, Ring polymer ranging C78 to C400 and linear polymer ranging C50 to C400 (united-atom model) (b) $\langle R_g^2 \rangle_{\text{linear}}$ and $\langle R_g^2 \rangle_{\text{ring}}$ in *NVT* MD simulation, both ring and linear polymer range 30 to 200 (Kremer-Grest bead)

Figure 3.1.3 (a) Linear polymer $g_{\text{inter}}(r)$ of C78 and C400 (united-atom model) with *NVT* MD (b) Ring polymer $g_{\text{inter}}(r)$ of C78 and C400 (united-atom model) with *NVT* MD (c) Linear polymer $g_{\text{inter}}(r)$ ranging 30 to 150 (Kremer-Grest model) with *NVT* MD (d) Ring polymer $g_{\text{inter}}(r)$ ranging 30 to 150 (Kremer-Grest model) with *NVT* MD

Figure 3.1.4 (a) Relaxation time in *NVT* MD simulation, Ring polymer ranging C78 to C400 and linear polymer ranging C50 to C400 (united-atom model) (b) Relaxation time in *NVT* MD simulation, both ring and linear polymer range 30 to 200 (Kremer-Grest bead)

Figure 3.1.7 (a) Diffusion coefficient in *NPT* MD simulation, these figure were maded using Hur et al. [ref] ring polymer ranging C40 to C1500 and linear polymer ranging C40 to C512 (united-atom model) (b) Diffusion coefficient in *NVT* MD simulation, both ring and linear polymer range 30 to 200 (Kremer-Grest bead)

Figure 3.2.1 Chain distribution of range (a) C50 to C500 ring (b) C300 to C500 ring (c) C50 to C500 linear (d) C50 to C500 linear with united-atom model in monolayers, Chain distribution of range (d) 50 to 200 ring (e) 50 to 200 with Kremer-Grest model in strict 2D

Figure 2.2.2 (a) Torsional Auto correlation (b) distribution of bond length (c) distribution of bond bending (d) distribution of torsional angle, in *NVT* MD with monolayer

Figure 3.2.3 (a) $\langle R_g^2 \rangle_{\text{ring}}$ in *NVT* MD with monolayer, Ring polymer ranging C50 to C500 (united-atom model) (b) $\langle R_g^2 \rangle_{\text{ring}}$ in *NVT* MD in strict 2D, Ring polymer range 30 to 400 (Kremer-Grest bead)

Figure 3.2.4 (a) Linear polymer $g_{\text{inter}}(r)$ of C50 and C250 (united-atom model), *NVT* MD with monolayer (b) Ring polymer $g_{\text{inter}}(r)$ of C50 and C250 (united-atom model), *NVT* MD with monolayer (c) Linear polymer $g_{\text{inter}}(r)$ ranging 30 to 150 (Kremer-Grest model) ,*NVT* MD in strict 2D (c) Ring polymer $g_{\text{inter}}(r)$ ranging 30 to 150 (Kremer-Grest model) , *NVT* MD in strict 2D

Figure 3.2.5 (a)Relaxation time in *NVT* MD simulation, Ring polymer ranging C78 to C400 and linear polymer ranging C50 to C400 (united-atom model) (b) Relaxation time in *NVT* MD simulation, both ring and linear polymer range 30 to 400 (Kremer-Grest bead)

Figure 3.2.6 (a) Diffusion coefficient in *NVT* MD with monolayer, Ring polymer ranging C50 to C500 (united-atom model) (b) Diffusion coefficient in *NVT* MD in strict 2D, Ring polymer range 30 to 400 (Kremer-Grest bead)

Figure 3.3.1 (a) C400 (united-atom model) in *NVT* MD, Blue chain get tangled by surrounding chains (b) After 3.76 ns, Blue chain escaped from surrounding chains

I. Introduction

Polymers generally have a broad spectrum of intrinsic time and length scales. These characteristics make polymeric materials possess both solid-like behaviors in short time scales and liquid-like behaviors in long time scales, i.e., viscoelastic properties. These peculiar characteristics of polymers have attracted a wide scientific and industrial interests.¹⁻⁴

As the microscopic molecular approaches to predict various rheological properties of polymer, the Rouse model well described the rheological properties of short-chain polymer melts.^{5,6} In contrast, rheological behaviors of long, entangled polymer melt systems have been successfully predicted by the reptation or tube theory originally developed by de Gennes, Edwards, and Doi.¹ Owing to tremendous research efforts⁷⁻¹⁰ over the years, a significant progress in the knowledge of entangled polymer melts has been achieved. However, as the reptation theory requires the existence of chain ends, it cannot describe the dynamics of ring polymers which have no chain ends, thus raising a new challenge in the field of polymer rheology.

There appeared numerous experimental and simulation works to understand the dynamics of ring polymers and quantify their rheological properties. Obtaining a pure unknotted and unconcatenated ring melt is very challenging in experiment due to an extreme difficulty to completely remove a linear contamination, thus having led to controversial experimental results in the past.¹¹⁻¹³ This problem can be overcome in computer simulations, as one can perfectly control the molecular architecture. Suzuki et al.¹⁴ observed Flory's exponent 1/3 for long ring polymers with bond fluctuation model (BFM). Hur et al.¹⁵ and Halverson et al.¹⁶ simulated up to C1500 atomistic ring polyethylene (PE) melts and 1600 Kremer-Grest ring bead melts, respectively. However, the dynamics and molecular mechanisms of ring polymers have not yet been well understood.

In this work, we studied in detail the general characteristics of ring dynamics in 2D as well as 3D systems. The paper is organized as follows: In Sec. II, we describe the molecular models and simulation methodology. Various dynamic and structural properties of ring polymer in 3D systems are presented in Sec. III 1 and the corresponding analysis of 2D systems is given in Sec. III 2. We provide a prediction of large ring dynamics in 3D systems in Sec. III 3. Section IV summarizes the present work.

II. Simulation method

2.1 United-atom model

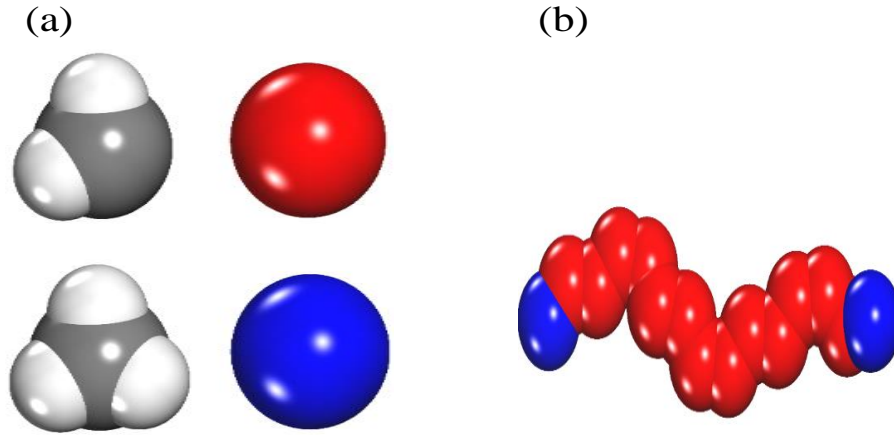


Figure 2.1.1 (a) Red atom represents united-atom1 (CH₂) and blue atom represents united-atom2 (CH₃). (b) Polymer chains are connected by bonded and non-bonded interactions such as bond-stretching, bond-bending, bond-torsional, and 6-12 Lennard-Jones potentials.

Canonical (*NVT*) MD simulations were carried out based on Newton's equations of motion implemented with the Nosé–Hoover thermostat.¹⁷⁻²⁰ These equations of motion have the following form:⁶

$$\dot{\mathbf{q}}_{ia} = \frac{\mathbf{p}_{ia}}{m_{ia}}$$

$$\dot{\mathbf{p}}_{ia} = \mathbf{F}_{ia} - \zeta \mathbf{p}' \quad (2-1)$$

$$\dot{\zeta} = \frac{P_{\zeta}}{Q}, \quad \dot{p}_{\zeta} = \sum_i \sum_a \frac{\mathbf{p}_{ia}^2}{m_{ia}} - dNk_B T, \quad Q = dNk_B T \tau^2 \quad (2-2)$$

In eq 1, q_{ia} , p_{ia} , F_{ia} , and m_{ia} are the position vector, momentum vector, force vector, and mass of atom a of the i^{th} -molecule. d indicates the dimension of space and N is the total number of atoms of system. Q , ζ , and p_ζ are the mass, position, momentum variables of the Nosé–Hoover thermostat.

For efficiency and accuracy in the simulation, the equations of motion were integrated using the reversible Reference System Propagator Algorithm (r-RESPA), allowing for two different time scales in simulation step: 2.35 fs for bond-stretching, bond-bending, and bond-torsional interactions, and 0.47 fs for non-bonded Lenard-Jones (LJ) interactions.²¹

The SKS united-atom model²² was employed in all the simulations. Figure 2.1.1 (a) shows visualization of the united-atom and polymer chain which use united-atom model and intramolecular potentials. The 6-12 LJ potential was adopted for non-bonded atom-atom interactions as follows.

$$U_{\text{LJ}}(r_{ij}) = 4\varepsilon_{ij} \left[\left(\frac{\sigma_{ij}}{r_{ij}} \right)^{12} - \left(\frac{\sigma_{ij}}{r_{ij}} \right)^6 \right] \quad (2-3)$$

The LJ parameters for the united-atoms are set as $\sigma = 3.93 \text{ \AA}$ and $\varepsilon/k_B = 47 \text{ K}$ for united-atom1 (CH_2), and $\sigma = 3.93 \text{ \AA}$ and $\varepsilon/k_B = 114 \text{ K}$ for united-atom2 (CH_3). The parameters ε_{ij} and σ_{ij} were calculated by the Lorentz-Berthelot mixing rule:

$$\varepsilon_{ij} = (\varepsilon_i \varepsilon_j)^{1/2}, \quad \sigma_{ij} = \frac{(\sigma_i + \sigma_j)}{2} \quad (2-4)$$

The three bonded (bond-stretching, bond-bending, and bond-torsional) interactions are described as follows. The bond-stretching interaction is represented by a harmonic potential function:

$$U_{\text{str}}(l) = \frac{k_{\text{str}}}{2} (l - l_{\text{eq}})^2 \quad (2-5)$$

where the equilibrium bond length $l_{\text{eq}} = 1.54 \text{ \AA}$ and the bond-stretching spring constant $k_{\text{str}}/k_B = 452,900 \text{ K/\AA}^2$. The bond-bending interaction is also expressed by a harmonic potential:

$$U_{\text{ben}}(\theta) = \frac{k_{\text{ben}}}{2} (\theta - \theta_{\text{eq}})^2 \quad (2-6)$$

where the equilibrium bending angle is $\theta_{eq} = 114^\circ$ and the bending constant $k_{ben}/k_B = 62,500 \text{ K/rad}^2$. The bond-torsional potential was originally developed by Jorgensen et al:²³

$$U_{torsional}(\phi) = \sum_{m=0}^3 a_m \cos^m \phi \quad (2-7)$$

where $a_0/k_B=1010\text{K}$, $a_1/k_B=2019\text{K}$, $a_2/k_B=136.4\text{K}$, and $a_3/k_B=-3165\text{K}$.

2.2 Kremer-Grest model

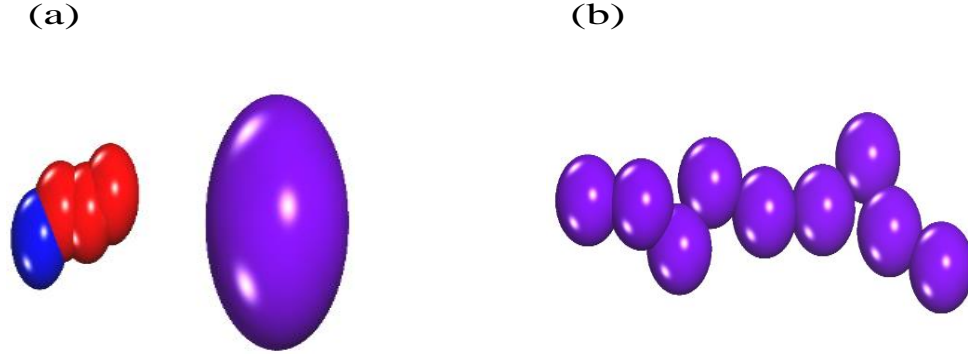


Figure 3.2.1 (a) Purple bead represents a Kremer-Grest bead accounting for 3~4 CH₂ united atoms in polyethylene molecule. (b) A Kremer-Grest chain is connected through the FENE and WCA potentials.

The *NVT* MD simulations were further carried out in both 3D and confined 2D systems using Newton's equations of motion with the Dissipative Particle Dynamics (DPD) thermostat.^{24,25} These equations of motion were described by following expressions:

$$\dot{\mathbf{q}}_{ia} = \frac{\mathbf{p}_{ia}}{m_{ia}}$$

$$\dot{\mathbf{p}}_{ia} = \mathbf{F}_{ia}^c + \mathbf{F}_{ia}^d + \mathbf{F} \quad (2-8)$$

In eq 1, \mathbf{q}_{ia} , \mathbf{p}_{ia} , and m_{ia} are the position vector, the momentum vector, and the mass of atom a of the i^{th} -molecule, respectively. In the Kremer-Grest model²⁶, \mathbf{F}_{ia}^c consists of both the shifted LJ (WCA) and the finitely extensible nonlinear elastic (FENE) potentials. A Kremer-Grest coarse-grained bead represents about 3 ~ 4 united atoms. Figure 2.2.1 (a) shows the visualization of coarse-graining. These equations of motion were integrated using the velocity Verlet method with a time step 0.01τ .

The WCA potential is given as

$$U_{WCA}(r_{ij}) \begin{cases} 4\varepsilon \left[\left(\frac{\sigma}{r_{ij}} \right)^{12} - \left(\frac{\sigma}{r_{ij}} \right)^6 \right] + \varepsilon, & r_{ij} \leq 2^{1/6} \sigma \\ 0, & r_{ij} \geq 2^{1/6} \sigma \end{cases} \quad (2-9)$$

The FENE potential is described as

$$U_{FENE}(r_{ij}) \begin{cases} -0.5kR_0^2 \ln \left[1 - \left(\frac{r_{ij}}{R_0} \right)^2 \right], & r_{ij} \leq R_0 \\ \infty, & r_{ij} \geq R_0 \end{cases} \quad (2-10)$$

Where $k = 30\varepsilon / \sigma^2$, $R_0 = 1.5\sigma$. In this model, bond length of equilibrium l_0 is about 0.96σ .

The standard reduced units were used in simulation: All physical quantities were expressed in terms of σ , m , and ε . All beads interact with each other via the WCA and FENE potentials as shown in figure 2.2.1 (b).

2.3 Simulation details

Table 1 Description of the simulated systems. Here M denotes the number of molecules in system, N the number of atoms (or beads) per molecule. Each system consists of monodisperse polymer chains.

Systems	M	N	Box length X	Box length Y	Box length Z
United-atom model	100	50	189.51 Å	189.51 Å	6.48 Å
in monolayer	100	100	260.84 Å	260.84 Å	6.48 Å
	100	150	317.10 Å	317.10 Å	6.48 Å
	100	250	407.64 Å	407.64 Å	6.48 Å
	100	500	575.55 Å	575.55 Å	6.48 Å
Kremer-Grest in	400	30	31.67(31.55) σ	21.11(21.03) σ	21.11(21.03) σ
linear (ring) 3D	160	50	21.11(21.03) σ	21.11(21.03) σ	21.11(21.03) σ
	160	70	29.56(29.44) σ	21.11(21.03) σ	21.11(21.03) σ
	120	100	31.67(31.55) σ	21.11(21.03) σ	21.11(21.03) σ
	80	150	31.67(31.55) σ	21.11(21.03) σ	21.11(21.03) σ
	135	200	31.67(31.55) σ	31.67(31.55) σ	31.67(31.55) σ
Kremer-Grest in	30	30	38.73 σ	38.73 σ	0
ring 2D	50	50	64.55 σ	64.55 σ	0
	70	70	90.37 σ	90.37 σ	0
	100	100	129.10 σ	129.10 σ	0
	150	150	193.65 σ	193.65 σ	0
	200	200	258.20 σ	258.20 σ	0



Figure 2.2.2 (a) Realistic wall where wall atoms are successively connected to each other at a specified distance. (b) Ideal smooth wall where wall atoms are connected to each other at an infinitely short distance. (c) Polymer chains are confined in-between the top and the bottom ideal smooth walls.

Initial configurations of systems were prepared using the Materials Studio software package.²⁷ We imposed the WCA potential in both the upper and bottom z -axes which act as ideal smooth wall. Figure 2.2.2 shows the feature of the ideal smooth wall in comparison with the realistic wall. After being confined by two ideal smooth walls, the initial configuration of system was prepared in an isothermal-isobaric (NPT) statistical ensemble using the Nosé–Hoover thermostat and barostat.

After equilibration of the initial system configuration, the system density was converged and selected for subsequent NVT MD simulations. Figure 2.3.1 shows the converged density profile as a function of chain length. These results were also used for choosing a proper density for 2D Kremer-Grest model systems.

Each system was simulated more than 10 times longer than its longest relaxation time. To make unknotted and unconcatenated ring configurations with the Kremer-Grest model of 3D systems, we built a system configuration in 2D and stack up the 2D configuration until the simulation box was completely filled with chains at the specified density. For efficient equilibration, we applied a soft potential²⁶ whose strength became increased gradually during a initialization step. After equilibration, the soft potential was replaced by the actual WCA potential. A similar procedure was used in constructing 2D ring systems.

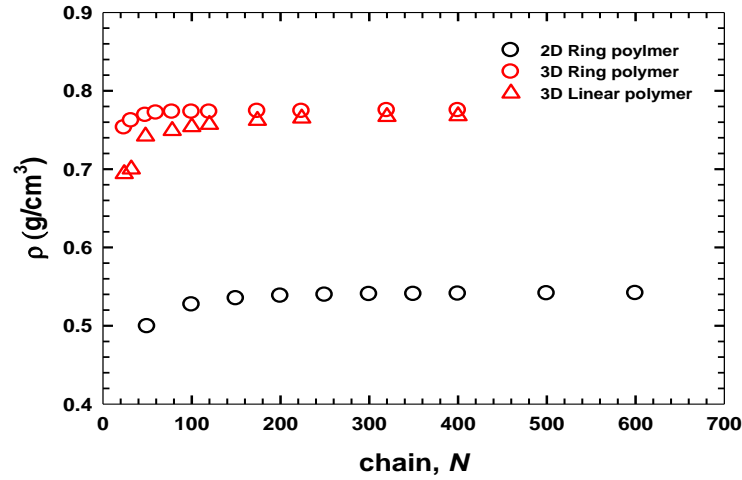


Figure 2.3.1 Density of the simulated ring melts. 2D ring systems converge between 0.5~0.6 values which are smaller than those of 3D systems.

For *NVT* MD simulations for ring systems with the Kremer-Grest model, we adjusted the system density as corresponding to that based on the united-atom model. Both the linear and ring systems using 3D Kremer-Grest model used the same density as $\rho = 0.85 \sigma^{-3}$ while the ring systems using 2D Kremer-Grest model adopted $\rho = 0.6 \sigma^{-3}$. Simulation details are described in Table 1. Snapshots of atomic configurations of the Kremer-Grest 2D model system were displayed in figure 2.3.2.

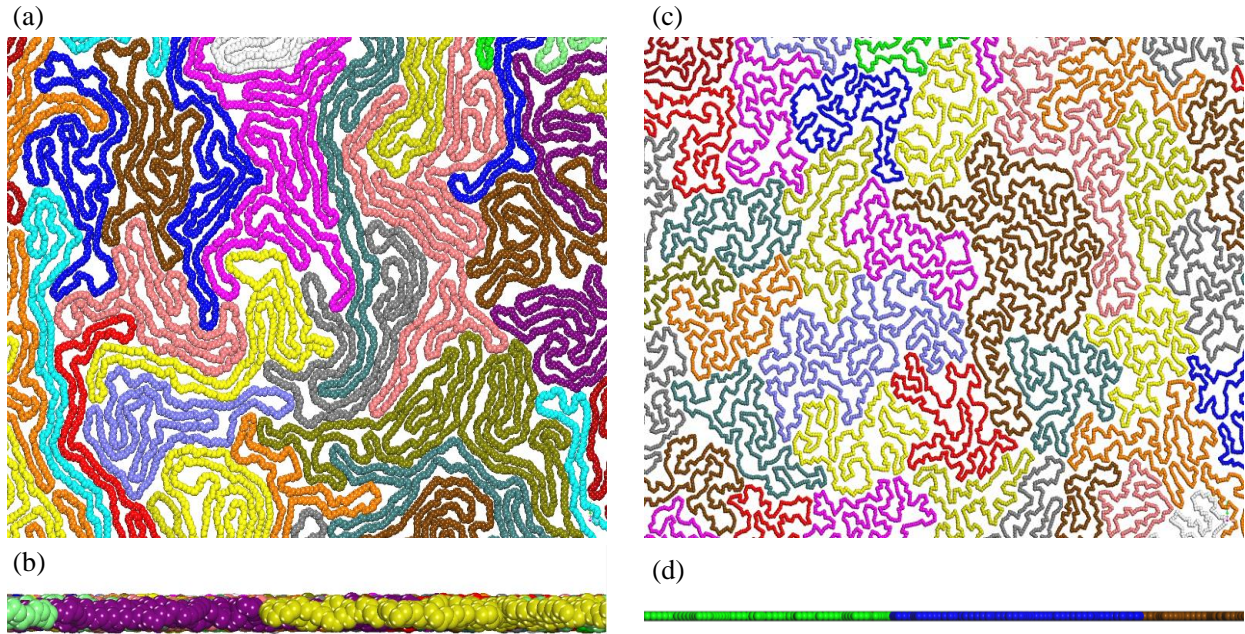


Figure 2.3.2 Snapshots of projected onto (a) xy -plane and (b) xz -plane for a ring melt using the united-atom model. Corresponding ones of (c) xy -plane and (d) xz -plane for a ring melt using Kremer-Grest model in 2D.

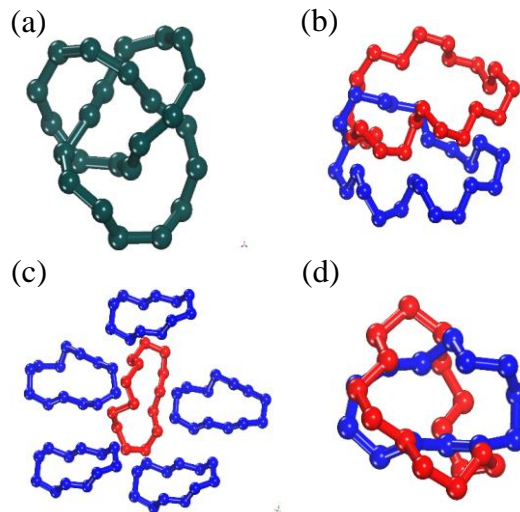


Figure 2.3.3 Ring configurations: (a) Knotted structure, (b) concatenated structure, (c) collapsed structure, and (d) penetrated structure.

The Knotted and concatenated structures are presented in Figure 2.3.3 (a) and (b). These configurations were completely excluded in the simulations. Respecting unknotted and unconcatenated ring structures, we picture two different ways in molecular arrangement for ring melts, distinct from the linear analogues: One is a collapsed configuration and the other one is a penetrated configuration.

III. Results and discussion

3.1 Static and dynamic properties in 3D comparing with linear polymer

The mean square chain radius of gyration of polymer can be described by a scaling behavior with respect to the number of atoms (beads) in the form of

$$\sqrt{\langle R_g^2 \rangle} \sim N^\nu \quad (3-1)$$

where ν is Flory's scaling exponent.^{1,2,6,14} Regardless of the molecular architecture, both the linear and ring polymer melts have $\nu=1/2$ when chain lengths are short enough for applying the Rouse model.^{1,5,6} As the chain length increases, ring polymer's ν value becomes smaller than $1/2$ value due to the constraints of ring topology. Cate and Deutsch³⁴ showed that ν value for ring polymer would converge to $2/5$ based on a Flory-like self-consistent theory. Suzuki et al. reached a conclusion that the ν value approaches $1/3$ with a modified self-consistent theory.¹⁴

The modified self-consistent theory in 3D evaluates the free energy per ring polymer in melt systems by taking into account an entropic penalty of polymer chain and an osmotic pressure from the neighboring chains. For simplicity, we denote $\sqrt{\langle R_g^2 \rangle}$ as R . The free energy $F(N, R)$ per ring polymer in melt systems is described as:

$$F(N, R) \sim F(N, R)_{osm} + F(N, R)_{ent} \quad (3-2)$$

$$\sim \frac{1}{N} \left[\frac{1}{R^2} \left(\frac{4\pi}{3} R^3 - N \right) \right]^2 R^2 + \frac{N}{R^2} \quad (3-3)$$

We can obtain the minimum value of the free energy at $dF(N, R)/dR = 0$, leading to

$$\frac{dF(N, R)}{dR} \sim \frac{64\pi^2 R^3}{9N} - \frac{4N}{R^2} - \frac{8\pi}{3} = 0 \quad (3-4)$$

From equation (3-4), we can obtain a scaling relationship between R and N :

$$R \sim N^{1/3} \quad (3-5)$$

From this result, we can conclude that Flory's exponent of ring systems in 3D will approach to 1/3.

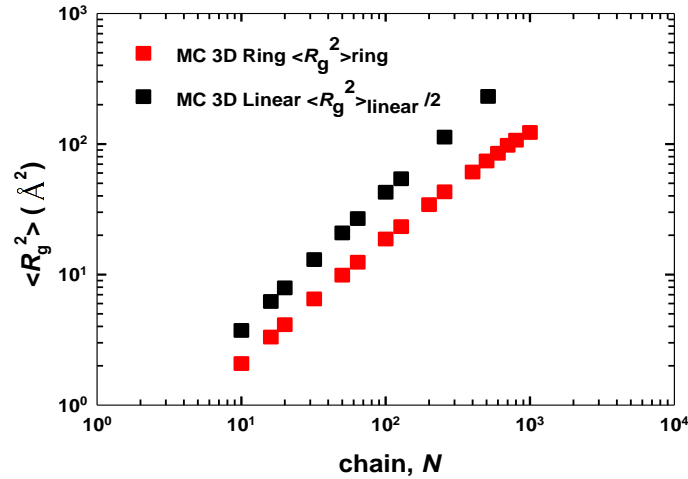
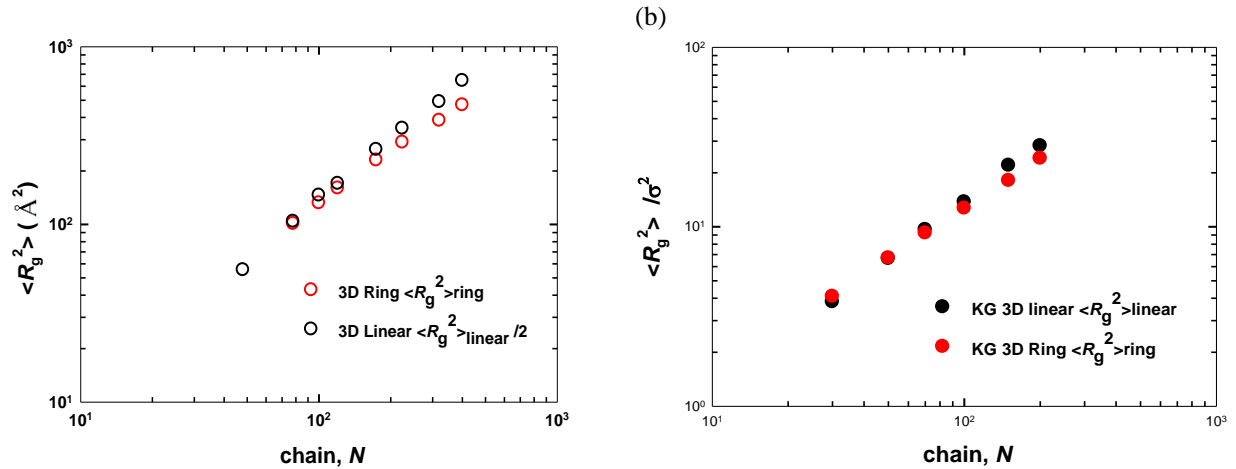


Figure 3.1.1 Results¹⁴ for $\langle R_g^2 \rangle_{\text{linear}}$ and $\langle R_g^2 \rangle_{\text{ring}}$ in *NVT* MC simulations. Ring polymers ranging from 10 to 1000 beads and linear polymers ranging from 10 to 512 beads.

Figure 3.1.1 shows the results of Suzuki et al.¹⁴ This results were calculated using *NVT* Monte Carlo simulation with the bond fluctuation model (BFM).²⁸⁻³⁰ The ν value of ring polymer approaches 0.365 when the number of beads is equal to 1000.

Figure 3.1.2 (a) $\langle R_g^2 \rangle_{\text{linear}}$ and $\langle R_g^2 \rangle_{\text{ring}}$ in *NPT* MD simulation; ring polymers ranging from C78 to C400

and linear polymer ranging from C50 to C400 (united-atom model) (b) $\langle R_g^2 \rangle_{\text{linear}}$ and $\langle R_g^2 \rangle_{\text{ring}}$ in NVT MD simulation; both ring and linear polymers range from 30 to 200 (Kremer-Grest) beads.



MD simulations were also carried out to understand dynamics of ring polymers in melt. We simulated both the united-atom model and the Kremer-Grest model systems. The chain length was in intermediate regimes so the ν value is higher than 1/3. The results displayed in Figure 3.1.2 shows that ν slightly decreases with increasing chain length. Other studies using MD simulations show a similar behavior to our result.^{15,16} The longer chains would be necessary for analyzing large ring polymer dynamics.

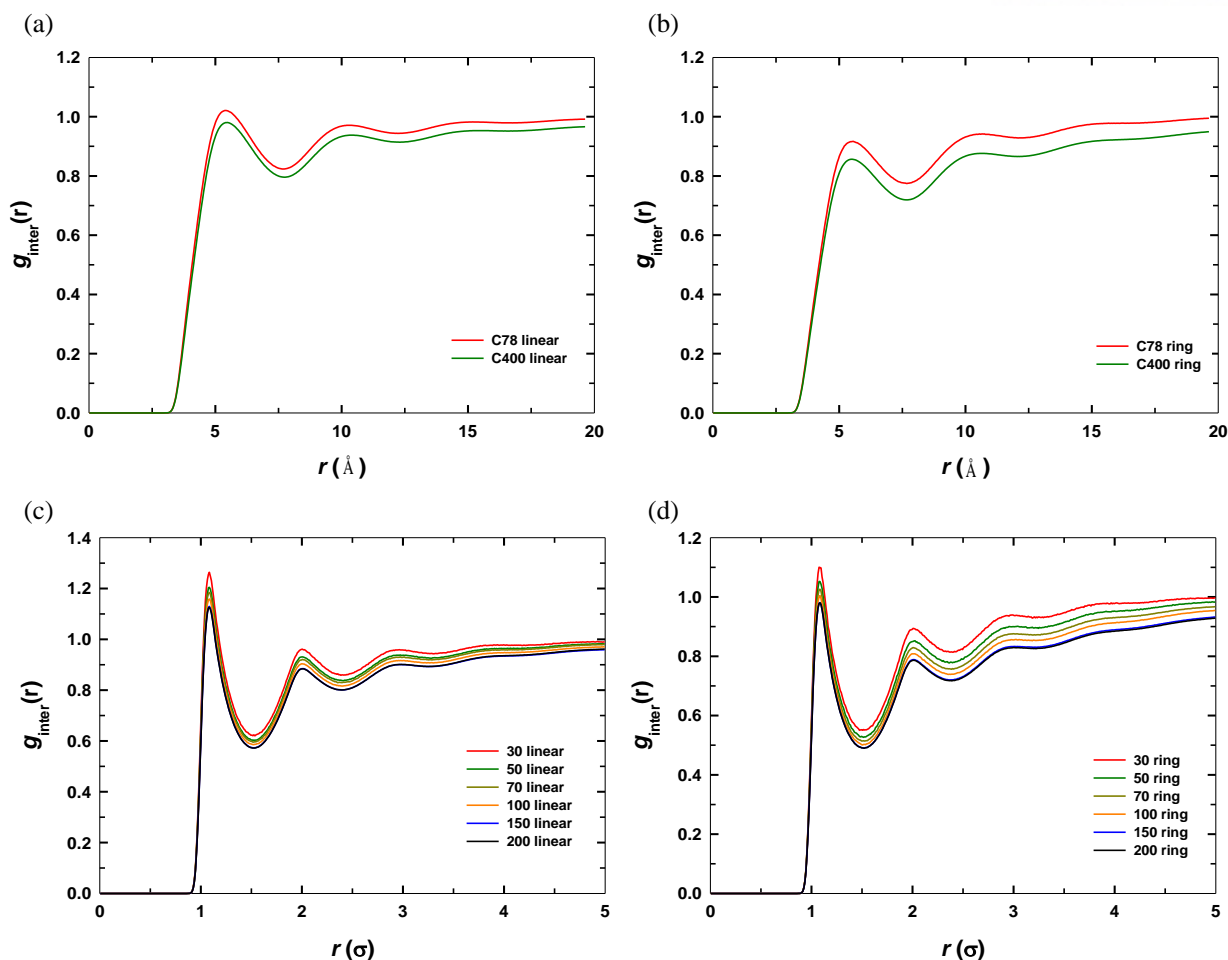


Figure 3.1.3 (a) Linear polymer $g_{inter}(r)$ of C78 and C400 (united-atom model) using *NVT* MD simulations. (b) Ring polymer $g_{inter}(r)$ of C78 and C400 (united-atom model) using *NVT* MD simulations. (c) Linear polymer $g_{inter}(r)$ ranging from 30 to 150 (Kremer-Grest model) using *NVT* MD simulations. (d) Ring polymer $g_{inter}(r)$ ranging from 30 to 150 (Kremer-Grest model) using *NVT* MD simulations.

Figure 3.1.3 represents the intermolecular radial distribution function $g_{inter}(r)$ for linear and ring polymer melts based on the united-atom model and the Kremer-Grest models. The two models employed the same number of atoms (beads) for the corresponding linear and ring analogues. $g_{inter}(r)$ of ring polymers is found to be always smaller than that of the linear analogues.

These results show that ring polymers have strong correlation in individual chain structure. The gap

between different chain lengths of intermolecular radial distribution are more sharply changed in ring melts with both united-atom model and Kremer-Grest model. These results may be evidence for a collapsed structure of ring polymers in melt.

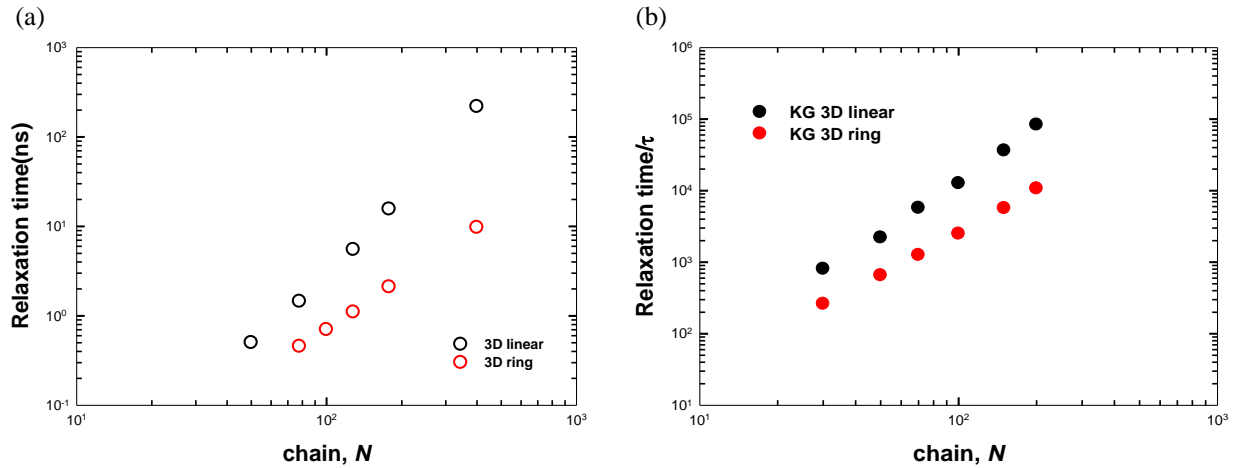


Figure 3.1.4 (a) Relaxation time in *NVT* MD simulation; ring polymers ranging from C78 to C400 and linear polymers ranging from C50 to C400 (united-atom model). (b) Relaxation time in *NVT* MD simulation, both ring and linear polymer range from 30 to 200 (Kremer-Grest bead)

The longest relaxation time of system is related with stress relaxation and viscosity. Long entangled linear polymers are well-known to exhibit a plateau regime in stress relaxation and 3.4 power law in viscosity and the longest relaxation time.

These results had proven by many experiments and simulations. Our simulation data also confirm this behavior in the case of linear polymers. Both linear and ring polymers follow the Rouse model in a short chain length regime. Beyond this regime, linear polymers follow the general feature of 3.4 power law. However, ring polymer systems do not exhibit the same behavior as linear systems. Ring polymers maintain the Rouse-like behavior with a slight larger value than 2.0 of the scaling exponent. These well-known ring properties were also proved by measuring stress relaxation.^{12,13}

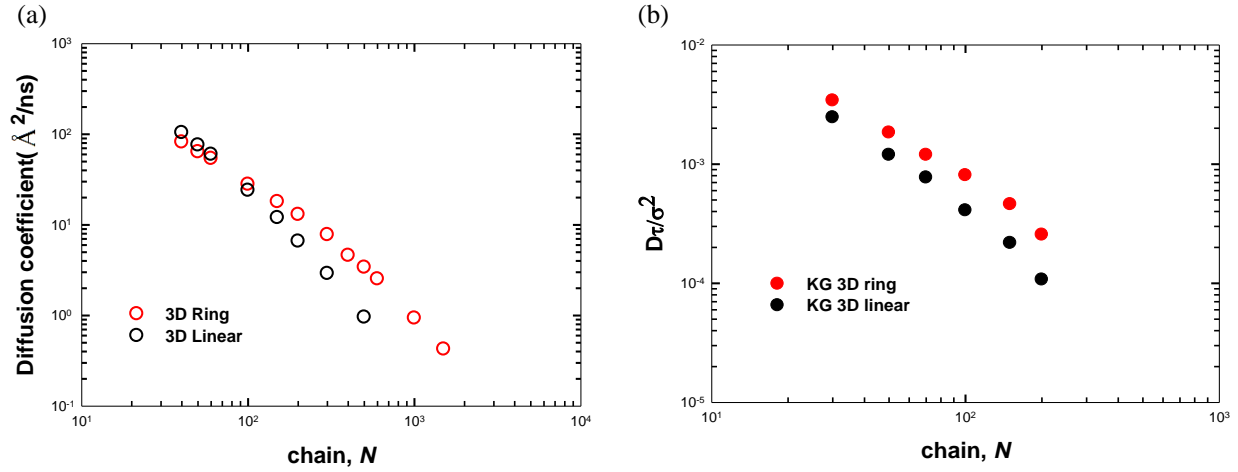


Figure 3.1.7 (a) Diffusion coefficient in *NPT* MD simulations by Hur et al.¹⁵ for ring polymers ranging from C40 to C1500 and linear polymer ranging from C40 to C512 (united-atom model). (b) Diffusion coefficient in *NVT* MD simulation for ring and linear polymers range from 30 to 200 (Kremer-Grest bead).

Linear polymers in melt systems exhibit a relation between the chain center-of-mass diffusion coefficient and stress relaxation time from the Rouse to the reptation regimes. The diffusion coefficient can be described by the following relations:

$$D_{cm} \sim \langle R_g^2 \rangle / \tau_{longest} \quad (3-6)$$

$$D_{cm} \sim N / N^2 \sim N^{-1}, \quad \text{For Rouse regime} \quad (3-7)$$

$$D_{cm} \sim N / N^{3.4} \sim N^{-2.4}, \quad \text{For entangled regime} \quad (3-8)$$

These relations cannot be applied to ring polymers. While the stress relaxation of ring system follows a Rouse-like behavior, the chain center-of-mass diffusion coefficient follows the scaling of entangled linear systems.

The chain length was not long enough to analyze dynamics of very large ring polymers with being characterized as 1/3 for the ν value. These results match with ring polymer of intermediate chain lengths. In the intermediate regime in chain length, penetration between ring chains is considered to make an important effect in ring dynamics.³¹

3.2 Structural and dynamic properties in monolayer and strict 2D

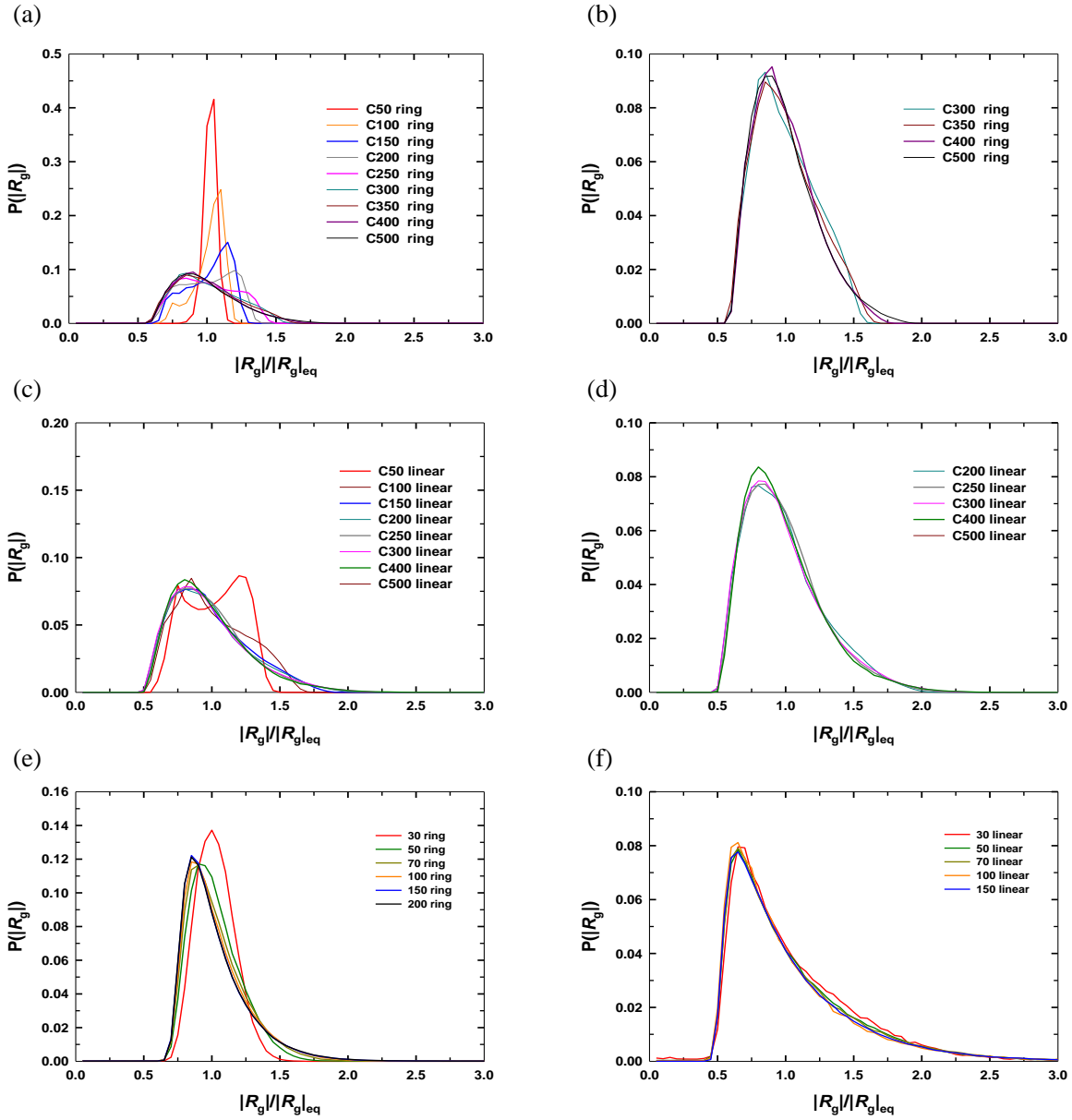


Figure 3.2.1 Probability distribution of the mean square chain radius of gyration for ring and linear melts: (a) C50 to C500 ring, (b) C300 to C500 ring, (c) C50 to C500 linear, (d) C50 to C500 linear polymers, based on the united-atom model in monolayers. The corresponding results for (e) 30 to 200 ring and (f) 30 to 200 linear polymers, based on the Kremer-Grest model in confined 2D

We designed MD simulations in monolayer and confined 2D systems for understanding the collapsed structural effect with excluding the ring penetration effect. Several properties were calculated for the systems. We maintain other properties being same for 3D system. We calculated proper densities for each simulation and simulated *NVT* MD using both United-atom model with monolayer and Kremer-Grest model in 2D.

Figure 3.2.1 show Probability distribution of the mean square chain radius of gyration for linear and ring polymers in monolayer and confined 2D. Linear and ring polymers of short chain length in monolayer show a non-Gaussian distribution. On the other hand, linear and ring polymers in confined 2D show nearly similar distribution regardless of chain length except for 30 ring system. There are several reasons for these results. First, the monolayer systems adjusted by *NPT* MD simulations find an appropriate density for ($T=450\text{K}$ and $P=1\text{ atm}$), so short chain systems have lower density. Second, chains are stiffer by restriction of the bond-bending and bond-torsional interactions, so a longer length scale between atoms are needed for eliminating a correlation between atoms. We selected chains which have a similar distribution for understanding ring polymer dynamics in 2D collapsed system.

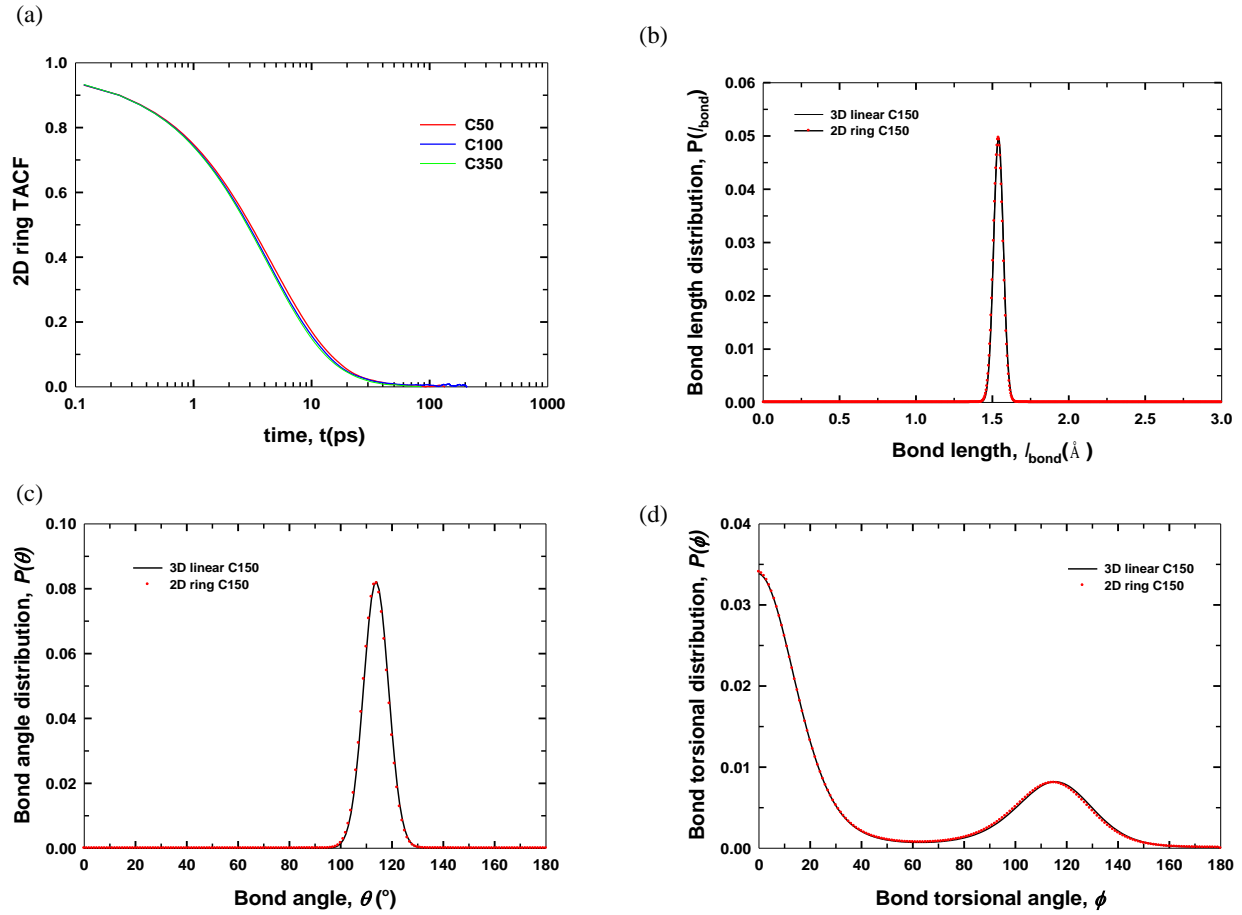


Figure 4.2.2 (a) Torsional Auto correlation (b) distribution of bond length (c) distribution of bond bending (d) distribution of torsional angle, in *NVT* MD with monolayer

We eliminated the z -dimension in confined 2D Kremer-Grest model systems. In contrast, the monolayer systems with the united-atom model were allowed for moving in the z -direction. We checked the system properties in small length and time scales for justifying the validity of our simulation systems. Figure 3.2.2 shows torsional auto correlation functions of 2D systems which exhibit a similar behavior to that of the 3D systems. As chain length increases, the relaxation time is shown to decrease and converge in about 5ps in ring polymers. Distributions of bond length, bond angle, and bond torsional appear very close to 3D simulation. These result demonstrates that the monolayer does not influence behaviors of polymer in very small length and time scales.

For calculating the ν value when the collapsed effect reaches a maximum like 1/3 in 3D, we slightly changed the modified self-consistent theory¹⁴ for 2D. We calculated the free energy per ring polymer in melt systems with considering only an osmotic pressure from the neighboring molecules. The total free energy $F(N, R)$ for ring polymer in melt systems as:

$$F(N, R) \sim F(N, R)_{osm} \quad (3-9)$$

$$\sim \frac{1}{N} \left[\frac{1}{R} (\pi R^2 - N) \right]^2 R \quad (3-10)$$

We can obtain the minimum value of the free energy at $dF(N, R) / dR = 0$, as described by:

$$\frac{dF(N, R)}{dR} \sim \frac{6\pi R^2}{N} - \frac{N}{R^2} - 2\pi = 0 \quad (3-11)$$

From equation (3-11), we can obtain the R and N relationship:

$$R \sim N^{1/2} \quad (3-12)$$

From this result, we can conclude the maximum ν value as 1/2 in 2D

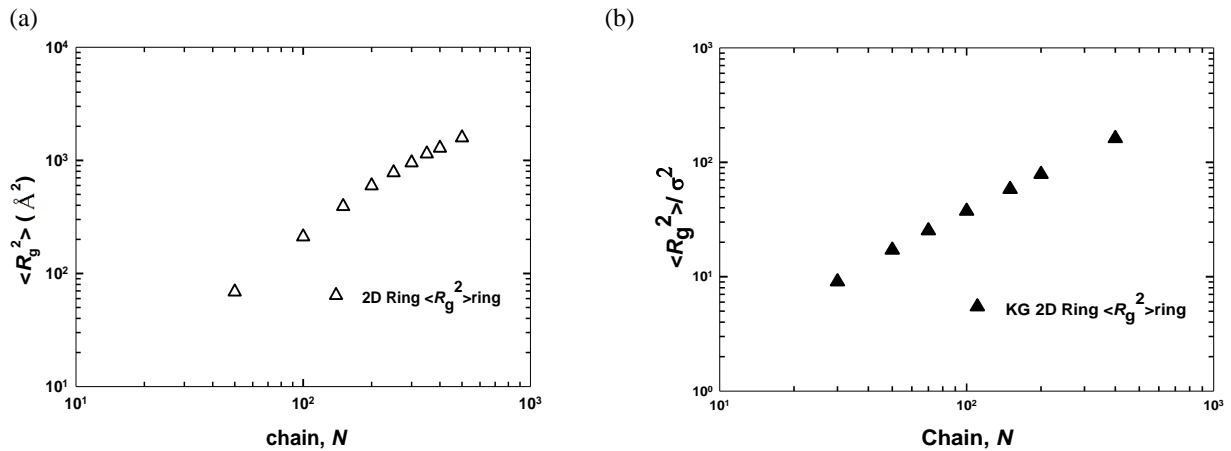


Figure 3.2.3 (a) $\langle R_g^2 \rangle_{ring}$ in NVT MD with monolayer; ring polymer ranging from C50 to C500 (united-atom model). (b) $\langle R_g^2 \rangle_{ring}$ in NVT MD in confined 2D; ring polymer range from 30 to 400 (Kremer-Grest bead)

Figure 3.2.3 shows both monolayer systems and confined 2D systems. Confined 2D systems exhibit $1/2$ for ν . Monolayer systems are not perfect 2D system, so these systems have slightly lower value than $1/2$. The ν values were converged in very short chain length regime as compared with 3D systems. This result presents that 2D systems has more dominant collapsed effect than 3D systems. All chains in 2D can be considered 100% collapsed, so the analysis of 2D ring systems may show a similar behavior of very long 3D 100% collapsed ring polymers.

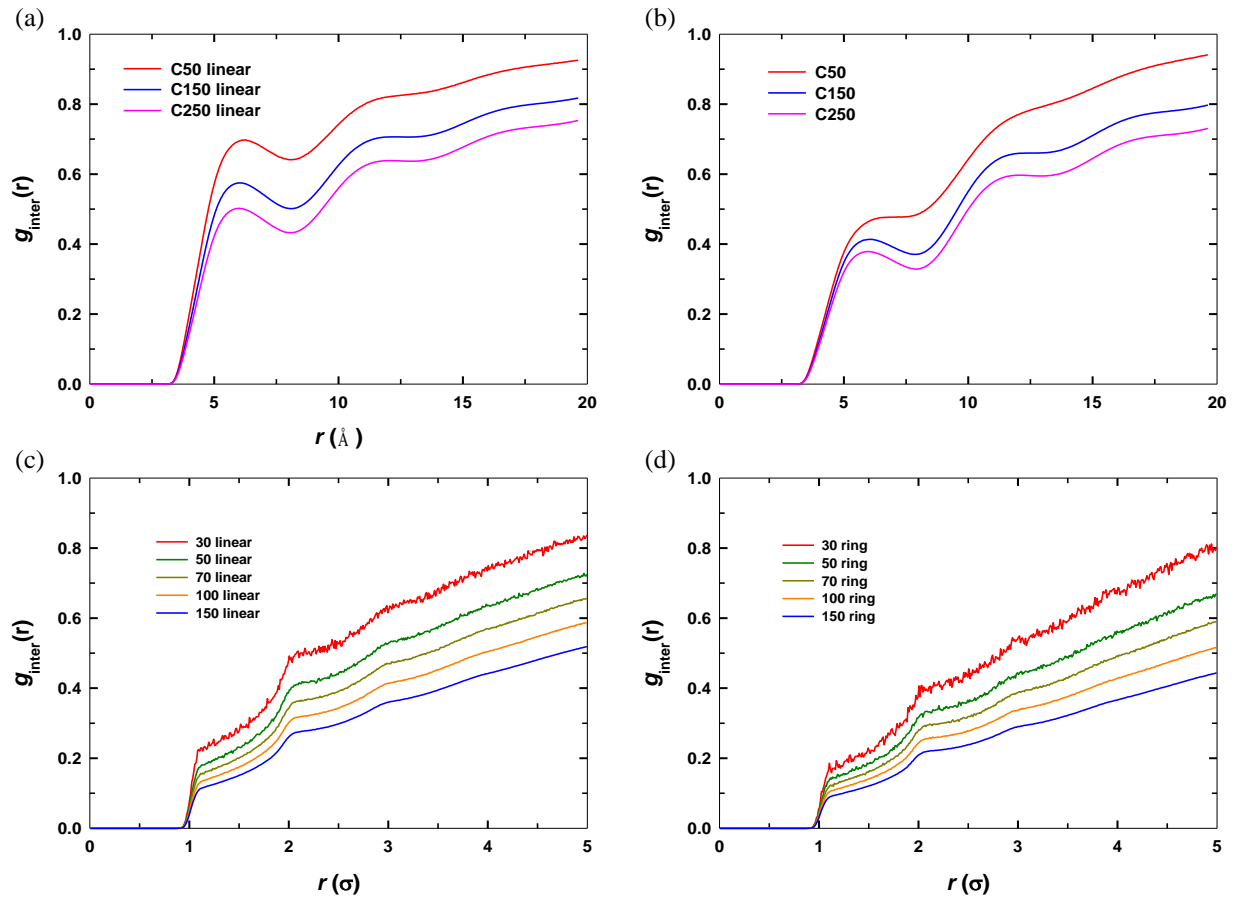


Figure 3.2.4 (a) Linear polymer $g_{inter}(r)$ of C50 and C250 (united-atom model), NVT MD with monolayer. (b) Ring polymer $g_{inter}(r)$ of C50 and C250 (united-atom model), NVT MD with monolayer. (c) Linear polymer $g_{inter}(r)$ ranging 50 to 150 (Kremer-Grest model), NVT MD in strict 2D. (d) Ring polymer $g_{inter}(r)$ ranging 50 to 150 (Kremer-Grest model), NVT MD in strict 2D

Monolayer and confined 2D intermolecular radial distributions are displayed in figure 3.2.4. The two model systems use the same number of atoms (beads) for comparing between linear and ring polymers. The intermolecular radial distribution of 2D systems exhibits a different shape than that of 3D case. The curves of ring polymers are shown to be below those of the counterpart linear ones as 3D systems. In 2D systems, the collapsed effect appears regardless of molecular architecture, so the gap in the intermolecular radial distribution between different chain length polymers are found to be similar for both linear and ring systems.

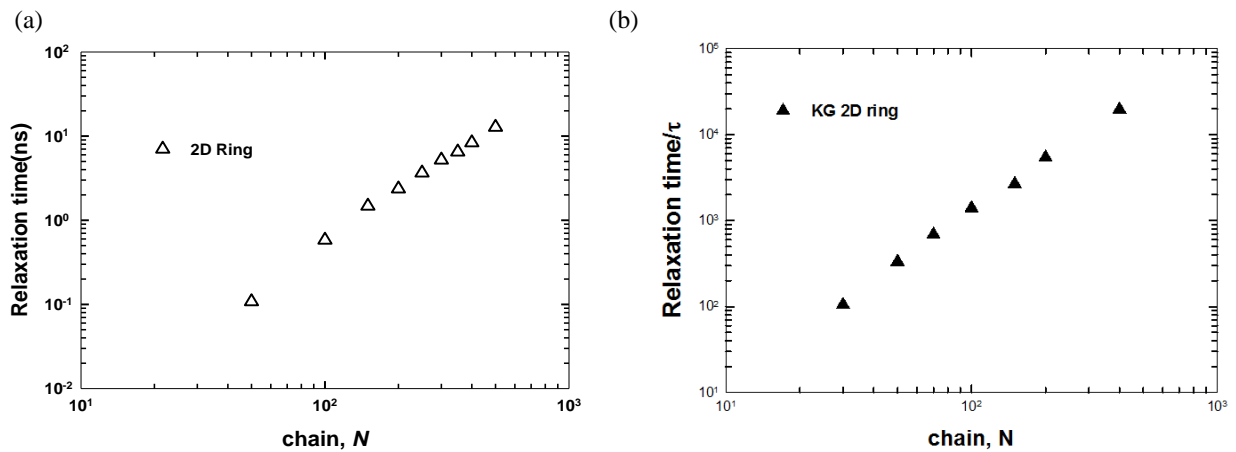


Figure 3.2.5 (a) Relaxation time in *NVT* MD simulation; ring polymer ranging from C78 to C400 and linear polymer ranging from C50 to C400 (united-atom model). (b) Relaxation time in *NVT* MD simulation, both ring and linear polymer range from 30 to 400 (Kremer-Grest bead)

Figure 3.2.5 presents results of the longest relaxation time for both monolayer and confined 2D systems. These results follow the Rouse-like scaling. 3D ring polymers in an intermediate range of chain length show a similar behavior with slightly larger scaling exponent. The scaling of the longest relaxation time in 2D ring polymers exhibits the following form:

$$\tau \sim N^\alpha, \quad \alpha \approx 2 \quad (3-13)$$

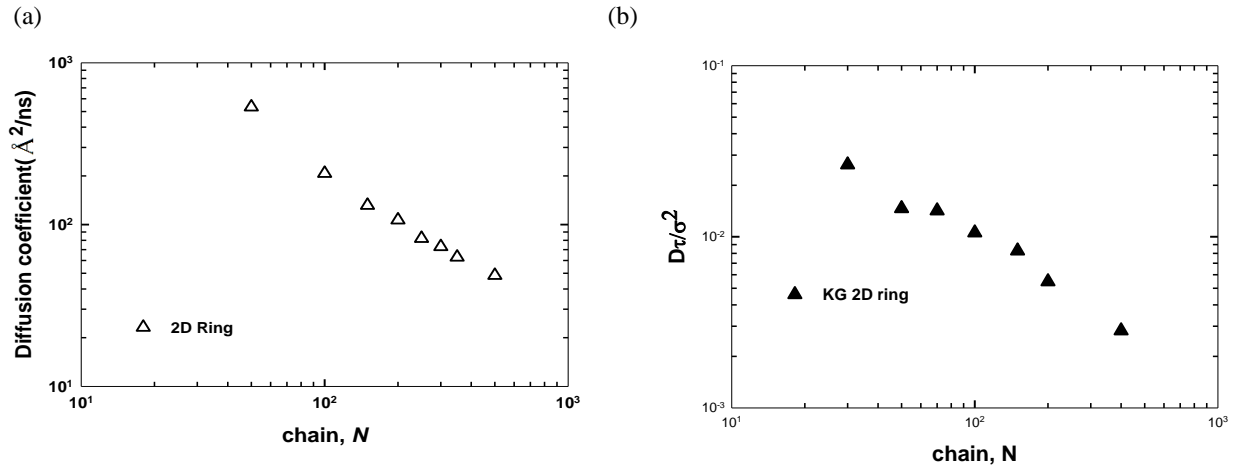


Figure 3.2.6 (a) Diffusion coefficient in *NVT* MD with monolayer; ring polymer ranging from C50 to C500 (united-atom model). (b) Diffusion coefficient in *NVT* MD in confined 2D; ring polymer ranging from 30 to 400 (Kremer-Grest bead)

The chain center-of-mass diffusion coefficient is shown in figure 3.2.6. While the diffusion coefficient of monolayer systems does not require a special treatment, the confined 2D systems need to account for the finite size effect.³⁵ Both diffusion coefficients show a similar behavior. The scaling of these coefficients is significantly different from an intermediate 3D scaling. The relation between atoms (beads) and self-diffusion coefficient can be expressed as:

$$D_{cm} \sim N^\beta, \quad -1 \leq \beta \quad (3-14)$$

3.3 Expectation of 3D large ring polymer dynamics

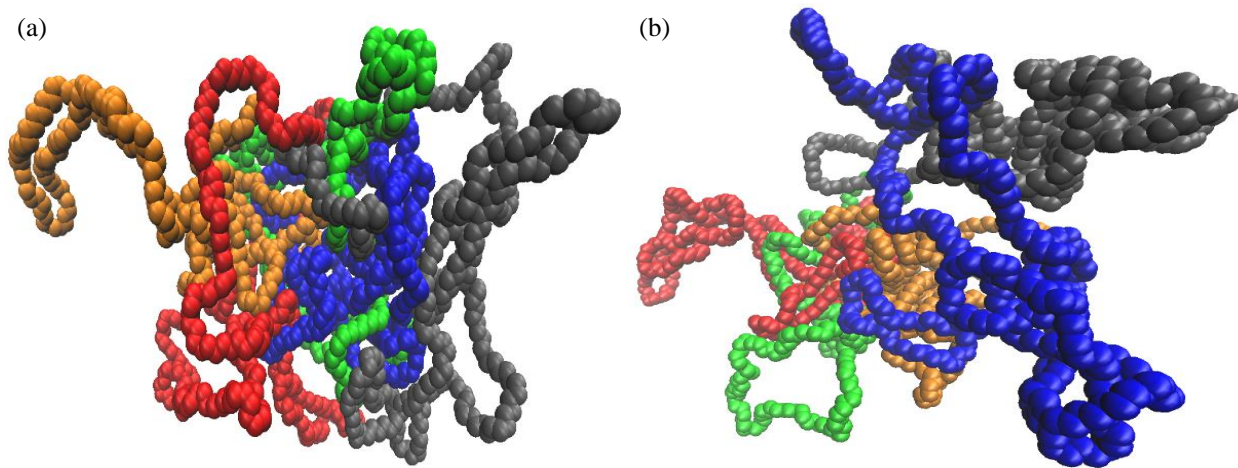


Figure 3.3.1 (a) C400 (united-atom model) in NVT MD; a blue chain gets tangled by surrounding chains. (b) After 3.76 ns, the blue chain has escaped from the surrounding chains

The results of 2D ring polymer in melt show significantly different behavior in the chain center-of-mass diffusion behavior. We do not yet understand a detailed molecular mechanism of ring polymer in intermediate and very long regimes of chain length. Penetration effect is also considered to be important for the intermediate regime of chain length as mentioned above. Figure 3.3.1 (a) shows that a ring (blue) chain is tangled with other surrounding chains. Figure 3.3.1 (b) shows that the blue chain has escaped from the surrounding chains after a certain time. The time required for the escape was found to be widely varied. The quantification of the penetration time scale is challenging, so additional works are needed.^{32,33}

The collapsed effect makes a contribution to decreasing Flory's exponent ν value and penetration effect makes a contribution in the opposite way to the collapsed effect. The result of 3D ring polymer in melt systems show that Flory's exponent ν value would reach $1/3$ as the chain length increases. At this length regime, the penetration effect is nearly negligible and dynamics of ring polymers is determined only by the collapsed effect. As such, the 2D simulation results can be useful in making a prediction for very long 3D ring polymer dynamics.

I. Conclusions

The molecular architecture differences of ring polymer gives rise to the topological constraint effects. These topological effects make ring polymer dynamics different from linear polymer dynamics. The present work can be summarized into three main findings. First, the Flory's exponent value for collapsed structures is $1/2$ in 2D melt systems even for small chain lengths. Second, the longest relaxation time has a Rouse-like scaling behavior of $\tau \sim N^\alpha$, $\alpha \approx 2$. Finally, the self-diffusion coefficient has an abnormal scaling behavior of $D_{cm} \sim N^\beta$, $-1 \leq \beta$

In future work, we will focus on the collapsed effects in 3D system by considering several different systems. We can easily make collapsed 3D systems by using modified bond repulsive potential which prevents penetration between chains. Adding an additional collapsed potential toward the chain center of mass is also a good way of making an effective collapse. Quantifying the effect of collapse on the self-diffusion coefficient would be important. Simple 2D systems can be useful in studying molecular mechanisms of ring polymers in melts.

Acknowledgments

This work was supported by the National Research Foundation of Korea (NRF-2013R1A1A2007749)

Computational resources were provided by the UNIST Super Computer Center.

References

- (1) Doi, M ; Edwards, S.F The theory of polymer dynamics; Oxford University Press; New York, 1986.
- (2) Rubinstein, M.; Colby, R. H. Polymer Physics; Oxford University Press: New York, 2003.
- (3) Bird, R. B.; Armstrong, R. C.; Hassanger, O. Dynamics of Polymeric Liquids, 2nd ed.; John Wiley and Sons, Inc.: New York, 1987; Vols. 1 and 2.
- (4) Morrison, F. A Understanding Rheology; Oxford University Press; New York 2001.
- (5) Rouse, P. E. J. Chem. Phys. 1953, 21, 1272.
- (6) Tsolou, G.; Stratikis, N.; Baig ,C.; Stephanou, P.S.; Marvranzas, V.G. Macromolecules 2010, 43, 10692.
- (7) McLeish, T. C. B. Adv. Phys. 2002, 51, 1379.
- (8) Watanabe, H. Prog. Polym. Sci. 1999, 24, 1253.
- (9) Graessley, W. W. Adv. Polym. Sci. 1974, 16, 1.
- (10) McLeish, T. C. B. Nat. Mater. 2008, 7, 933.
- (11) Roovers, J. Macromolecules 1988, 21, 1517.
- (12) Kapnistos, M.; Lang, M.; Vlassopoulos, D.; Pyckhout-Hintzen, W.; Richter, D.; Cho, D.; Chang, T.; Rubinstein, M. Nat. Mater. 2008, 7, 997.
- (13) Doi, Y.; Matsubara, K.; Ohta, Y.; Nakano, T. Macromolecules 2015, 48, 3140
- (14) Suzuki, J.; Takano, A.; Deguchi, T.; Matsushita, Y. J. Chem. Phys. 2009, 131, 144902.
- (15) Hur, K.; Jeong, C. Macromolecules 2011, 44, 2311.
- (16) Harverson, J. D.; Lee, W. B.; Grest, G. S.; Grosberg, A. Y.; Kremer, K. J. Chem. Phys. 2011, 134, 204905.
- (17) Nose, S. Mol. Phys. 1984, 52, 255.
- (18) Nose, S. J. Chem. Phys. 1984, 81, 511.
- (19) Nose, S. Prog. Theor. Phys. Supp. 1991, 103, 1.

- (20) Hoover, W. G. Phys. Rev. A. 1985, 31, 1695.
- (21) Martyna, G. J.; Tuckerman, M. E.; Tobias, D. J.; Klein, M. L. Mol. Phys. 1996, 87, 1117.
- (22) Siepmann, J. I.; Karaborni, S.; Smit, B. Nature 1993, 365, 330.
- (23) Jorgensen, W. L.; Madura, J. D.; Senson, C.J. J. Am. Chem. Soc. 1984, 106, 6638.
- (24) Groot, R. D.; Warren, P. B.; J Chem Phys 1997, 107, 4423.
- (25) Xu, X. I.; Chen, J. h. J Chem Phys 2014, 140, 174902.
- (26) Kremer, K.; Grest, G. S. J Chem Phys 1990, 92, 5057
- (27) Materials Studio, Accelrys Software Inc.: San Diego CA.
- (28) Brown.; Szamel, G. J Chem Phys. 1998, 109, 6184.
- (29) Brown.; Szamel, G. J Chem Phys. 1998, 108, 4705.
- (30) Shaffer, J. S.; Chem Phys. 1995, 103, 761
- (31) Lee, E. S.; Kim, S. R. Macromo.Rapid Commun. 2015, 10, 1002
- (32) Lang. M. Macromolecules. 2013, 46, 1158.
- (33) Tsalikis, D. G. Macro Letters. 2014, 3, 763.
- (34) Cates, M. E.; Deutsch, J. M. J. Phys. France. 1986, 47, 2121.
- (35) Semenov, A. N.; Meyer, H. Soft matter. 2013, 9, 4249